Evolution of condensed oxide at early and late stages of an aluminum particle combustion

Fabien Halter, Stany Gallier, Hugo Keck, Edward L. Dreizin, Christian Chauveau

Proceedings of the Combustion Institute 41 (2025) 105958

Contents lists available at ScienceDirect

Proceedings of the Combustion Institute

journal homepage: www.elsevier.com/locate/proci

Evolution of condensed oxide at early and late stages of an aluminum particle combustion

Fabien Halter [a,b,*], Stany Gallier [c], Hugo Keck [a,b], Edward L. Dreizin [d], Christian Chauveau [a]

[a] CNRS-ICARE, 1C Avenue de la Recherche Scientifique, 45380 Orléans, France
[b] University of Orléans, Château de la Source, 45100 Orléans, France
[c] ArianeGroup, Le Bouchet Research Center, Vert-le-Petit 91710, France
[d] New Jersey Institute of Technology, NJ 07102, Newark, USA

ARTICLE INFO

Keywords:
Aluminum particle
Alumina lobe
Particle covering
Particle spinning and jetting

ABSTRACT

This work provides new insights into the dynamics of the initial oxide lobe that forms from the native alumina layer covering an aluminum particle. This lobe is a distinctive hallmark of aluminum particle combustion — absent in hydrocarbon droplet combustion — and is commonly considered the origin of micrometric oxide residues. While it is generally accounted for in numerical simulations, this study challenges the prevailing assumption of its persistence. Instead, it demonstrates that the initial alumina lobe progressively regresses over time. The rate of this regression is closely linked to the availability of gaseous aluminum near the droplet surface and is notably delayed in nitrogen-containing environments. Moreover, this research offers a novel perspective on the final phase of the particle's combustion, which is initiated by the formation of a surface layer composed of alumina and/or oxynitrides. The presence of nitrogen plays a key role in triggering this covering process, which subsequently induces spinning and jetting phenomena. The study elucidates the mechanisms behind these dynamics — particularly jetting — and provides quantitative data on their effects in more complex configurations involving particle suspensions.

1. Introduction

Aluminum is widely employed as an energetic additive in solid rocket propellants and high explosives. More recently, it has garnered increasing attention as a potential source of carbon-free energy [1,2]. Previous studies on aluminum combustion have primarily focused on burn time and steady-state combustion regimes. It is now well established that large droplets burn predominantly in the vapor phase, while smaller droplets (typically in the 10–20 μm range) exhibit combustion limited by chemical kinetics [3,4]. The primary by-product of aluminum combustion is aluminum oxide (alumina, Al_2O_3). In vapor-phase combustion, alumina mainly forms as nanoparticles — commonly referred to as oxide smoke [5] — generated both in the detached flame zone and as a cap-like or lobe-shaped deposit on the surface of the burning particle. This surface lobe, originating from the native oxide shell of the solid particle, limits the area of exposed aluminum available for evaporation. As a result, it decreases the evaporation rate and extends the particle's burn time. This lobe is a distinctive feature of aluminum particle combustion, distinguishing it from the combustion of liquid hydrocarbons. It alters the local flow field by promoting the formation of hot, particle-bound regions rich in oxide smoke, thereby enhancing thermophoretic transport and further promoting lobe growth [6]. Once the aluminum core is fully consumed, the alumina lobe remains as a solid residue, often comparable in size to the original particle. These residual oxide particles can adversely affect the performance of solid rocket motors by contributing to two-phase flow losses when expelled through the nozzle [7]. The mechanisms governing the formation and evolution of the oxide lobe during combustion remain poorly understood. Despite its frequent observation, most insights are derived from post-combustion product analysis [8]. The final stages of aluminum particle combustion often exhibit unsteady dynamics, widely attributed to the presence of the oxide lobe. In summary, prior research has clearly demonstrated that the development of an alumina lobe significantly influences the combustion behavior and lifetime of aluminum particles. This study leverages ultra-resolved temporal and spatial visualizations of burning particles to provide new insights into: (i) the dynamic evolution of the oxide lobe during combustion, and (ii) the mechanisms underlying the final stages of particle burnout.

* Corresponding author at: University of Orléans, Château de la Source, 45100 Orléans, France.
E-mail address: fabien.halter@cnrs-orleans.fr (F. Halter).

https://doi.org/10.1016/j.proci.2025.105958
Received 11 July 2025; Accepted 15 October 2025

2. Methods

2.1. Description of the experimental set-up

The experimental apparatus has been described in detail in a previous work; the reader is referred to [9] for a comprehensive description. The experimental setup primarily consists of a high-pressure combustion chamber equipped with an electrostatic levitation system and a laser ignition device. Initially, pre-charged aluminum particles are introduced into the electric field at the center of the levitator. By adjusting the voltages applied to the electrodes, a single particle is trapped and positioned precisely at the focal point of the ignition laser. A CO_2 laser, operating at a wavelength of 10.6 μm with a power of 50 W, is used to ignite the particle. The levitated particle is symmetrically heated from both sides by a split laser beam. Laser emission duration is controlled via an external trigger activated by the light signal detected by photomultiplier tubes. The combustion chamber, which can operate up to 12 MPa, enables experiments under well-controlled gas-phase conditions with various atmospheric compositions. In this study, experiments are restricted to 1 bar gas mixtures containing 20% oxygen, diluted with argon, nitrogen, or a combination of both. Hereafter, the notation O_2/Ar refers to a binary mixture composed of 20% oxygen and 80% argon by volume. Similarly, O_2/N_2 denotes a mixture of 20% oxygen and 80% nitrogen. The aluminum powder used in these experiments is provided by Hermillon (France) and has a purity of 99.7%. The selected particles are sieved to obtain a size range between 50 and 100 μm. The temporal monitoring of the burning particle's evolution is performed using an imaging setup that combines a high-speed PHANTOM camera with a long-distance QUESTAR QM100 microscope, both focused on the reacting particle. A scale is provided in the figures presenting the images of burning particles. The initial particle diameter after melting is denoted by d_0. The reference time t_1 corresponds to the first displayed image, and all subsequent event times are given relative to this initial time.

2.2. Simulations

Direct numerical simulations of a single, spherical, burning aluminum droplet are carried out by solving the reactive Navier–Stokes equations in one-dimensional spherical coordinates around the droplet using an in-house code. The conservation equations for mass, momentum, energy, and chemical species are solved using a detailed kinetic mechanism for Al-O reactions, which includes 12 gas-phase reactions and 9 species. Numerical aspects, such as transport properties and kinetic data, are omitted here for conciseness and can be found in [9,10]. We here just recall that governing conservation equations are solved by a finite volume approach until steady-state. The oxide cap is not modeled explicitly. The liquid alumina ($Al_2O_{3(l)}$) smoke is treated as a standard gas-phase species, with the exception that its diffusion coefficient is set to zero ; its motion is instead governed by thermophoresis (see [9] for details). At the droplet surface, aluminum vaporization is described using a Hertz–Knudsen expression. Surface temperature and species mass fractions are determined by enforcing flux continuity conditions for both energy and mass at the interface. Within the liquid aluminum core, the model assumes no presence of gas-phase species and neglects thermal gradients, i.e., an isothermal behavior. No explicit surface chemical reactions are included for oxide formation; however, the condensation process $Al_2O_{3(l)} \rightarrow Al_2O_{3(cap)}$ is considered at the droplet surface, representing the deposition of alumina smoke from the gas phase onto the particle surface to form the oxide cap, noted $Al_2O_{3(cap)}$ in this document. The kinetics of this process are modeled using a sticking coefficient equal to one.

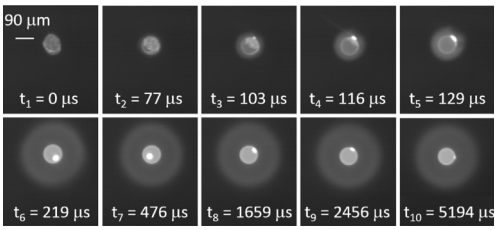

Fig. 1. Experimental evidence of alumina consumption. O_2/N_2, 1 bar, d_0 = 89 μm. The corresponding video is available in the supplementary material.

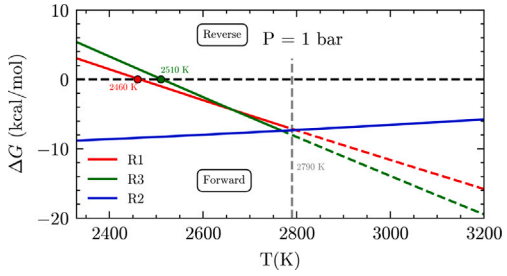

Fig. 2. Gibbs free energy for reactions (R1) to (R3).

3. Initial alumina consumption

3.1. Experimental evidence of the initial cap regression

A sequence of frames in Fig. 1 illustrates the progression of a particle toward thermal runaway when subjected to heating in an oxidizing atmosphere. Initially, the particle melts and adopts a spherical shape. It is coated with a thin native alumina layer (approximately 4 nm) [11]. As the temperature increases beyond 2500 K [12,13], the molten alumina reorganizes into one or more lobes that float on the particle surface (frames t_1 to t_5 in Fig. 1). Due to the immiscibility between liquid aluminum and alumina, as well as their differing optical emissivities, these distinct phases become clearly visible. It is important to note that the evaporation and/or dissociation temperature of alumina is typically estimated to exceed 4000 K at atmospheric pressure—well above the temperatures reached in these experiments. Traditionally, it is assumed that the alumina lobe grows through an oxide accumulation mechanism, though this process remains poorly characterized, as suggested by analyses of unburnt residues [14]. However, the present experimental observations reveal an initial decrease in the lobe's volume, a regression that is clearly visible in frames t_5 to t_{10} of Fig. 1. This phenomenon contrasts with conventional assumptions, and is observed in approximately 80% of the combustion cases in air. Prior studies have also noted that the size and persistence of the alumina lobe are sensitive to the surrounding gas composition, as discussed in the subsection *Influence of the gaseous environment*.

It is hypothesized that, at high temperatures and in fuel-rich environments — conditions likely to prevail just above the surface of an evaporating Al droplet — liquid alumina may undergo reduction. The two following global reactions are proposed as the most probable pathways:

$$4Al_{(l)} + Al_2O_{3(cap)} \leftrightarrow 3Al_2O_{(g)} \quad (R1)$$

$$4Al_{(g)} + Al_2O_{3(cap)} \leftrightarrow 3Al_2O_{(g)} \quad (R2)$$

The Gibbs free energies for these reactions are plotted in Fig. 2 at 1 bar (kcal by mole of aluminum). They are computed based on the evolution of enthalpy $H(T)$ and entropy $S(T)$ for each species taken from JANAF thermochemical database [15].

At temperatures near the boiling point of aluminum (2790 K), which are expected at the surface of the burning droplet, both reactions

Table 1
Calculated droplet temperature and Al partial pressure.

Diameter (μm)	T (K)	Al partial pressure
40	2440	0.12
50	2540	0.22
70	2575	0.31
100	2580	0.32

proceed spontaneously — that is, in the forward direction — resulting in the consumption of alumina. This thermodynamic analysis, which does not account for reaction kinetics due to the lack of available data in the literature, does not allow us to determine which of the two reactions is dominant. It is worth noting that reaction (R1) may reverse when the droplet temperature drops below 2460 K. In Fig. 2, the following additional reaction is also considered:

$$(2y - x)\,Al_{(l)} + Al_xO_yN_{z(l)} \leftrightarrow yAl_2O_{(g)} + \frac{z}{2}N_2 \quad (R3)$$

The discussion of reaction (R3) is postponed to Section *Alumina growth quenching the particle*, which addresses the formation of oxynitrides. The results of simulations performed for a 20% O_2 in N_2 mixture at $P = 1$ bar, and for various droplet diameters, are summarized in Table 1. A decrease in droplet temperature with decreasing diameter is observed, which is attributed to the reduction in aluminum partial pressure resulting from enhanced diffusion. As shown in Fig. 2, lower temperatures — associated with smaller droplets — favor oxide formation via reaction (R2). Indeed, ΔG then becomes positive, indicating that reaction is spontaneous in the reverse direction (oxide production). In contrast, larger droplets maintain higher temperatures, making reaction (R1) more likely to dominate and thus consume more oxide.

3.2. Influence of the gaseous environment

In certain cases, high-resolution visualizations enable the quantification of the lobe regression rate. However, movements of the lobe along the droplet surface can cause it to move out of the field of view, thereby preventing accurate tracking. When measurable, the regression rate is found to be approximately 1.5 times faster in an O_2/Ar mixture than in O_2/N_2—namely, 0.15 and 0.10 $mm^2\ s^{-1}$, respectively. These real-time observations are consistent with previously reported analyses of combustion residues. In O_2/Ar environments, Prentice [16,17] observed no alumina lobe, whereas it was present in O_2/N_2. Similarly, Dreizin [8] reported that the lobe was either absent or significantly smaller in O_2/Ar and O_2/He, but clearly visible in O_2/N_2. Comparable trends were also observed by Zenin et al. [18,19]. Simulations conducted in the present study for a 20% O_2 mixture in N_2 show no major differences when compared to the 20% O_2 in Ar case (at $P = 1$ bar and $d_0 = 70$ μm). This similarity is attributed to the comparable thermodynamic and diffusive properties of Ar and N_2. These findings strongly suggest that the differences observed experimentally are due to a chemical contribution from nitrogen. Dreizin [8] proposed that significant amounts of NO could be formed. Given its low reactivity, NO may diffuse toward the droplet surface and act as an oxygen carrier, promoting oxidation at the aluminum interface. To investigate this hypothesis, the kinetic mechanism was extended to include NO chemistry, introducing four additional species (N, NO, N_2O, NO_2) and six corresponding reactions. Reactions and rate coefficients are taken from GRI-Mech 3.0. Other nitrogen-containing species (e.g., NO_3, HONO, N_2O_5, etc.) may also form but were not considered here. The simulations confirm Dreizin's hypothesis, showing a peak in NO molar fraction in the vicinity of the droplet surface. The simulated molar fraction profiles are plotted in Fig. 3 as a function of the radial distance normalized by the droplet diameter (conditions: $P = 1$ bar, $d_0 = 70$ μm, $N_2/O_2 = 80/20$).

The NO concentration profile has been magnified by a factor of 10 for clarity. Its peak mole fraction is approximately 0.003 and, notably,

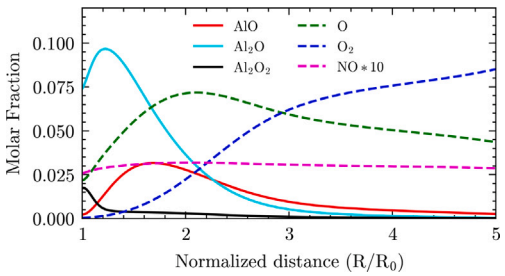

Fig. 3. Molar profiles of selected oxygen-bearing species as a function of the distance normalized by the droplet radius — NO profile is multiplied by 10 — 1 bar, O_2/N_2 (20/80), $d_0 = 70$ μm.

remains nearly constant across the normalized radial distance. This behavior reflects the fact that NO is formed at high temperatures in the reaction zone and diffuses back toward the droplet surface without being consumed in subsequent reactions. The concentrations of NO_2 and N_2O are significantly lower (on the order of 10^{-7}) and are thus not shown. At the droplet surface, atomic oxygen is present at a mole fraction of 2×10^{-2} and may undergo adsorption or reaction. The atomic nitrogen concentration at the surface is roughly two orders of magnitude lower. To explore the potential chemical role of NO, we considered a hypothetical surface reaction:

$$3NO_{(g)} + 2Al_{(l)} \rightarrow Al_2O_{3(cap)} + \frac{3}{2}N_{2(g)},$$

modeled with a high kinetic rate constant to simulate a fast process. Under conditions of $P = 1$ bar and $d_0 = 70$ μm, the simulation predicts a small but non-negligible surface oxide formation rate of $\dot{m}''_{Al_2O_3} = 0.024\ kg\ m^{-2}\ s^{-1}$, compared to an aluminum vaporization rate of $\dot{m}''_{Al} = 2.8\ kg\ m^{-2}\ s^{-1}$. Another plausible (thermodynamically favorable) pathway is the catalytic decomposition of NO on the particle surface (either on the bare aluminum or on the oxide lobe):

$$NO \rightarrow \tfrac{1}{2}O_2 + \tfrac{1}{2}N_2,$$

which would locally release oxygen capable of reacting with $Al_{(g)}$ in the near-surface region. This would decrease the concentration of available aluminum vapor and potentially suppress reaction (R2). Simulations incorporating surface reactions [10] further indicate that smaller droplets exhibit a higher surface coverage by adsorbed species — including nitrogen-containing ones — on the aluminum surface. Saturation of the surface with these species (mostly, monoatomic N) may hinder reaction (R1). The complete regression of the alumina lobe proceeds more rapidly in the O_2/Ar mixture due to ongoing reactions between alumina and aluminum (in both gas and liquid phases). These reactions generate gaseous suboxides such as Al_2O, which are transported away from the surface by the Stefan flow and contribute to lobe reduction. In contrast, the delayed regression observed in O_2/N_2 environments can be attributed to the back-diffusion of nitrogen oxides and their role in consuming aluminum vapor at the surface. Once the oxide lobe has fully disappeared, the aluminum droplet undergoes steady evaporation without any further observable phenomena, until a subsequent transition occurs.

4. Oxide cap & quenching

4.1. Evidence of the alumina growth

We define combustion Phase 1 as the ignition of the aluminum droplet. Phase 2 corresponds to the steady regression of the droplet, while Phase 3 begins with the onset of an asymmetric combustion regime. The steady regression phase concludes with the appearance of a rapidly expanding region on the droplet surface, which partially envelops the aluminum core (Fig. 4).

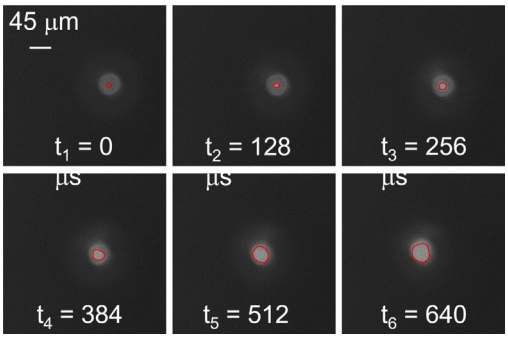

Fig. 4. Experimental evidence of the growing alumina cap. O_2/N_2, 1 bar, d_0 = 74 µm. (For interpretation of the references to color in this figure legend, the reader is referred to the web version of this article.)

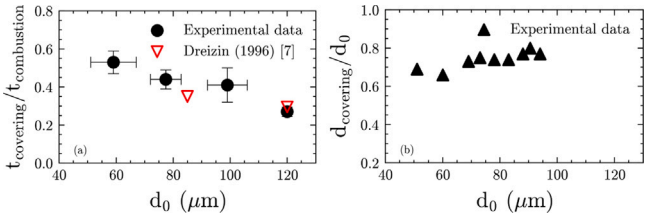

Fig. 5. Normalized cap appearance timing (a) and particle diameter for cap occurrence (b) as a function of the initial particle diameter, in air.

It grows at an approximate rate of 0.9 mm^2/s. This region, artificially highlighted in red in Fig. 4, corresponds to a newly formed condensed phase. Its visibility on the droplet surface is likely due to distinct optical properties. Fig. 4 captures the rapid expansion of this phase on the same 74-µm diameter droplet whose normalized light emission is presented in Fig. 6. The onset of this growth marks the beginning of combustion Phase 3, as indicated in Fig. 6. For the droplet with an initial diameter of 74 µm, this transition occurs when the particle diameter has decreased to approximately 40 µm. The new condensed phase is identified as alumina, forming a growing cap on the surface. The remainder of this study is devoted to investigating the origin of this sudden transition in the combustion dynamics.

4.2. Influence of the particle diameter and of the gaseous environment

In the case illustrated in Fig. 4, the onset of surface coverage occurs when the droplet diameter reaches 40 µm, corresponding to half of the initial diameter and approximately 70% of the initial aluminum mass. Simulations performed for various particle diameters (see Table 1) show a temperature drop of about 140 K when decreasing the droplet diameter from 100 to 40 µm. Notably, the calculated temperature for a 40-µm droplet is 2440 K, which lies below the inversion temperatures of reactions R1 and R3, as shown in Fig. 2. This suggests that the transition to Phase 3 could be triggered by the formation of liquid alumina on the droplet surface, resulting from the reversal of these two reactions. To test this hypothesis, a series of experiments were conducted in an O_2/N_2 environment, varying the initial droplet diameter (d_0 ranging from 50 to 120 µm). Fig. 5a presents the time of onset of oxide cap formation, denoted $t_{covering}$, normalized by the total combustion duration, as a function of the initial diameter. Data from Ref. [20] are included, showing excellent agreement with the present results. The extent of the oxide cap increases with particle size.

Our experimental results do not support the existence of a critical radius or a critical particle temperature, as such assumptions would imply a monotonic increase in the normalized covering time with increasing droplet diameter. This conclusion is further substantiated

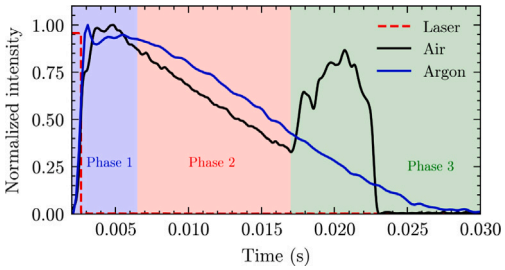

Fig. 6. Combustion intensity as a function of time, in air (black line) and O_2/Ar 80/20% vol. mixture (blue line). The signal from the CO_2 laser used for ignition is displayed (red dashed line) along with combustion phases for air. (For interpretation of the references to color in this figure legend, the reader is referred to the web version of this article.)

Table 2
Oxidizer impact on the oxide cap occurrence.

Mixture composition (with 20% O_2)	$d_{covering}/d_0$	$t_{covering}//t_{combustion}$
N_2 – 80%	0.74	0.46
N_2 – 60%/Ar – 20%	0.72	0.67
N_2 – 40%/Ar – 40%	0.63	0.71
N_2 – 20%/Ar – 60%	0.55	0.83
Ar – 80%	0.40	0.93

by Fig. 5b, which shows the evolution of the diameter at which the oxide cap appears, $d_{covering}$, normalized by the initial droplet diameter d_0. The increasing trend of this ratio with d_0 indicates that, for larger droplets, the end of the steady combustion phase occurs at a larger absolute diameter. This suggests that particle temperature alone cannot explain the transition. It is likely that in this case, thermophoresis can be a strong provider of oxide smoke towards the lobe [9]. Moreover, replacing nitrogen with argon significantly alters the phenomenology observed in the final stages of the particle's combustion. Specifically, the steady regression phase — during which the droplet diameter decreases smoothly — is considerably prolonged. This behavior is visually captured in Fig. 6, where the curve corresponding to the O_2/Ar mixture (blue) exhibits an almost monotonic evolution up to the final stages of combustion.

When using argon, the droplet cap forms only once the drop diameter decreases to approximately 10–15 µm, representing less than 2% of the mass of the initial 60 µm particle. Combustion in an O_2/N_2 environment (curve in black in Fig. 6) becomes unsteady at a much earlier stage. Table 2 lists both the onset time and the corresponding cap diameter for various ambient conditions. To further clarify the observed trends, additional experiments were conducted using argon in place of nitrogen. Substituting nitrogen with argon progressively extends the duration of the quasi-steady regression phase at smaller droplet diameters. The presence of nitrogen in the mixture promotes early droplet cap formation. To understand this contrasting behavior, we initially compared the thermal and diffusive properties of nitrogen and argon. The most significant difference lies in their heat capacities, which nearly double in the presence of nitrogen (1.35 kJ/(kg K) for nitrogen versus 0.6 kJ/(kg K) for argon, values computed near the droplet surface using the NASA-CEA code). However, the calculated droplet temperatures for these different mixtures are nearly identical. The following section investigates potential kinetic effects that may explain our experimental observations.

4.3. Discussion on the possible paths leading to the cap growth

The results presented in Table 2 further highlight the significant influence of N_2 compared to Ar, suggesting a chemical effect, as previously discussed in Section *Initial alumina consumption*. Nitrogen

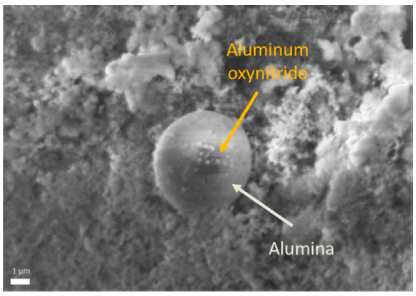

(a) Scanning electron microscope image of a large micrometric alumina particle with an aluminum oxynitride inclusion. O_2-21% / N_2-79%, 1 bar.

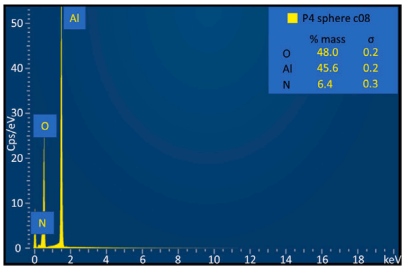

(b) Energy-dispersive X-ray spectroscopy of the large micrometric alumina particle with the identification of O, Al and N mass fractions.

Fig. 7. Experimental evidence of oxynitride formation during combustion of Al particles of average diameter $d = 7$ µm.

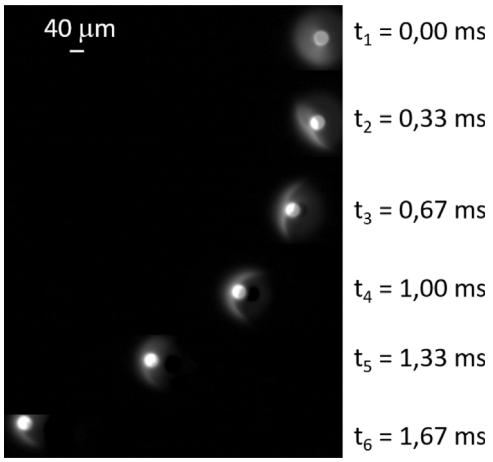

Fig. 8. Experimental evidence of jetting, O_2/N_2, 1 bar, $d_0 = 55$ µm.

may promote the formation of aluminum oxide from NO via surface reactions (see Section *Influence of the gaseous environment*). Moreover, evidence of aluminum oxynitride formation has been observed in quenched droplets burned in an O_2/N_2 atmosphere (see Fig. 7-top). In these cases, nitrogen is detected at the center of the alumina sphere, appearing as a darker region. Under these specific conditions (air at 1 bar), the EDX spectrum (Fig. 7-bottom) reveals an overall oxynitride composition of $Al_{1.7}O_3N_{0.5}$. Aluminum oxynitrides exhibit a wide homogeneity range, with an average stoichiometry of $Al_{23}O_{27}N_5$ (equivalent to $9Al_2O_3 \cdot 5AlN$), which melts congruently at 2440 K [21]. Fig. 2 shows the Gibbs free energy for reaction (R3), incorporating $AlON_{(l)}$ represented as $9Al_2O_3 \cdot 5AlN$. It is important to note that thermodynamic data for this liquid oxynitride are not available in the literature; thus, as a first-order approximation, it was modeled as a mixture of 9 $Al_2O_{3(l)}$ and 5 $AlN_{(l)}$. According to Fig. 2, the temperature for spontaneity of reaction (R3) shifts slightly upward—from 2460 K for pure oxide to 2510 K for the oxynitride. This suggests that oxynitride formation is favored at higher temperatures, and thus more likely in larger droplets. An alternative explanation may also involve direct nitride formation. The only thermodynamically spontaneous reaction at droplet temperatures is $Al_{(l)} + 0.5N_2 \rightarrow AlN_{(l)}$.

Experimental data in Fig. 5 indicate that the formation of the oxide cap depends on the initial droplet size. Larger aluminum droplets tend to transition earlier into the asymmetric regime, suggesting the development of a more pronounced lobe. This behavior is consistent with the thermophoresis mechanism described in [9], where both experimental and numerical results demonstrated that the presence of a small lobe — regardless of its chemical composition — induces a strong thermophoretic flux of oxide smoke from the surrounding flame. This flux rapidly nourishes the lobe due to the temperature gradient between the hotter surrounding gas and the cooler lobe, resulting in a net thermophoretic flow directed toward the lobe. A simplified zero-dimensional model has been proposed in [22] based on this mechanism, showing that larger droplets tend to form larger lobes. The ratio of lobe diameter to initial droplet diameter is found to be approximately 0.7–0.8, with a slight increase observed as the initial droplet size increases—consistent with the measurements in Fig. 5b. As surface reactions take place, it is hypothesized that aluminum oxide and aluminum oxynitride species may be adsorbed onto the aluminum particle. Once saturation is reached, the solubility of aluminum oxides and aluminum oxynitrides is reached and the subsequent addition of such species to the droplet's surface leads to the formation of a condensed phase on the particle surface. The saturation of these species on the droplet's surface is also linked to the collision frequency between these species. As the concentration increases, more collisions between these non-miscible species occur, that could lead to the formation of a nucleus, acting as a potential source for the formation of this condensed phase. This cap is then likely to enhance thermophoretic deposition, thereby accelerating oxide growth and the subsequent encapsulation of the particle.

4.4. Implications of the covering

A burning droplet that becomes partially covered with an inert surface layer (cap) is expected to experience translational motion due to a momentum imbalance between the evaporating aluminum surface and the non-evaporating, capped region. As a result, the droplet is propelled in the direction of the cap. This phenomenon is referred to as *jetting* throughout the remainder of this paper. Fig. 8 illustrates the abrupt onset of this motion, marked by the appearance of a bright spot — indicative of oxide formation — at the lower left corner of the aluminum droplet at time t_1. As the oxide layer spreads over a larger portion of the droplet surface, the droplet moves simultaneously in the same direction as the growing cap. This behavior is consistently observed across all experiments, confirming that the droplet's motion is linked to a Stefan flow deficit on the coated side, which creates a net momentum imbalance. Fig. 8 also captures the rapid displacement of the particle immediately following the appearance of the oxide spot, a consequence of the high surface coverage rate (approximately 1 mm^2/s).

Spinning may result from the sliding of the oxide cap once the droplet begins to move, or from asymmetric gas release on the droplet surface, which can generate a torque. However, the spinning rate is expected to decrease over time due to viscous damping. The combination of spinning and jetting can lead to spiraling trajectories, a behavior frequently observed during experiments. As the lobe develops, the associated propulsive force increases, thereby enhancing jetting.

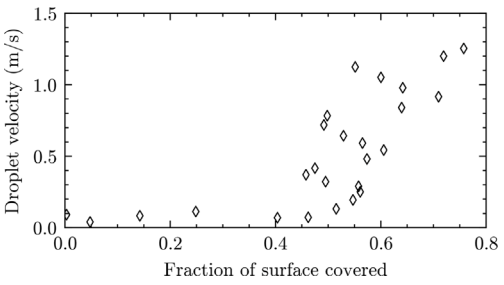

Fig. 9. Jetting velocity evolution with the fraction of the droplet covered by the oxide, O_2–20%/N_2–80%, 1 bar, $d_0 = 55$ μm.

Jetting is thus directly linked to the extent of the surface covered by the inert cap [23]. The available visualizations allow for accurate tracking of the droplet's position and estimation of the oxide-covered surface area. Based on this information, we approximate both the droplet velocity and the percentage of its surface that is coated, though the latter remains uncertain since only one side of the droplet is visible. It is assumed that both sides are coated symmetrically. Fig. 9 presents the evolution of droplet velocity as a function of the oxide coverage percentage, corresponding to the sequence shown in Fig. 8. Note that velocity changes are derived from two-dimensional imaging. However, since the particle remains in focus throughout the sequence, velocity components perpendicular to the camera plane are assumed negligible. Initially, the oxide-covered area increases up to approximately 50% of the droplet surface without significant motion. As previously discussed, the surface coverage rate is high, and this apparent delay in motion can be attributed to the droplet's inertia. This interpretation is supported by a classical inertial timescale estimation, given by $\rho d_0^2/18\ \mu$ (where ρ is the aluminum density and μ the gas viscosity), which yields approximately 3 ms—comparable to the typical coverage time of around 1 ms as seen in Fig. 8.

Following this initial phase, the oxide-covered area continues to grow, eventually reaching 80% of the droplet surface. This increasing momentum imbalance leads to particle acceleration, with velocities rising to 1–2 m/s. The terminal velocity cannot be determined, as the droplet eventually exits the field of view. These observations carry important implications for understanding and modeling the propagation of combustion waves in particle-laden gaseous media (e.g., explosions, burner-stabilized flames, etc.). It would be inaccurate to define a particle's thermal influence solely by the static temperature field surrounding a burning droplet. Mobile particles substantially extend their zone of influence, particularly in nitrogen-rich environments.

5. Conclusion

Experiments on aluminum particles (40–100 μm), laser-ignited at 1 bar in a gaseous environment, show that an oxide lobe forms upon melting and ignition, then vanishes as quasi-steady combustion begins. Instability arises when an oxide cap reforms and grows. Although this behavior was noted in Braconnier's thesis [24], the role of oxygen concentration remains under study. Results suggest that nitrogen affects both the disappearance of the initial lobe and the reformation of the oxide cap. A simplified thermodynamic and fluid dynamics model attributes this to NO_x species transporting oxygen to the aluminum surface, enhancing local oxidizer concentration and delaying oxide removal. Later, this same mechanism promotes the growth of a liquid oxide cap, possibly involving a liquid oxynitride phase. The overall influence of nitrogen is summarized in Table 3. The capping phase correlates with spinning and jetting, with particles at combustion's end reaching speeds above 1 m/s, potentially igniting nearby particles. Further research is required to assess the implications of these findings for solid rocket engines, where the operating environment differs significantly (high pressures and temperatures, other oxidizers).

Table 3
Summarized influence of nitrogen.

Reaction	Associated mechanism
$3NO_{(g)} + 2Al_{(l)} \rightarrow Al_2O_{3(cap)} + \frac{3}{2}N_{2(g)}$	Oxide cap growth from presence of NO near the droplet's surface.
$NO \rightarrow \frac{1}{2}O_2 + \frac{1}{2}N_2$	Presence of oxygen near the droplet's surface favored by NO decomposition, decreasing the importance of reaction (R2) through a decrease in available Al.
$Al_{(l)} + 0.5N_2 \rightarrow AlN_{(l)}$	Formation of aluminum nitrides that can further oxidize to form aluminum oxinitrides that can be adsorbed by the droplet.
$(2y - x)\,Al_{(l)} + Al_xO_yN_{z(l)} \leftrightarrow yAl_2O_{(g)} + \frac{z}{2}N_2$	Formation of aluminum oxinitrides that can be adsorbed by the droplet.

Novelty and significance statement

A phenomenological description of early combustion and burnout of a single aluminum droplet is proposed. This is a first novelty of this research since those two phases are often overlooked in previous works. Thanks to a recent and adequate set-up (levitator), new or hardly reported physics (e.g., oxide consumption, surface covering, particle jetting...) is unraveled, measured, and discussed. One finding is the strong role of nitrogen, which can no longer be considered as inert. The observed phenomena may alter aluminum combustion in terms of burn time, combustion efficiency, or particle trajectories, and could be significant in actual systems such as rocket motors or burners.

CRediT authorship contribution statement

Fabien Halter: Designed research, Analyzed data, Wrote the paper. **Stany Gallier:** Performed simulations, Analyzed data, Wrote paper. **Hugo Keck:** Performed experiments, Analyzed data. **Edward L. Dreizin:** Analyzed data. **Christian Chauveau:** Designed research.

Declaration of competing interest

The authors declare that they have no known competing financial interests or personal relationships that could have appeared to influence the work reported in this paper.

Acknowledgments

The authors declare that they have no known competing financial interests or personal relationships that could have appeared to influence the work reported in this paper. S.G. thanks the French Defense Procurement Agency DGA (Direction Générale de l'Armement) for funding.

Appendix A. Supplementary data

Supplementary material related to this article can be found online at https://doi.org/10.1016/j.proci.2025.105958.

References

[1] J.M. Bergthorson, Recyclable metal fuels for clean and compact zero-carbon power, Prog. Energy Combust. Sci. 68 (2018) 169–196.
[2] F. Halter, S. Jeanjean, C. Chauveau, Y. Berro, M. Balat-Pichelin, J.F. Brilhac, A. Andrieu, C. Schonnenbeck, G. Leyssens, C. Dumand, Recyclable metal fuels as future zero-carbon energy carrier, Appl. Energy Combust. Sci. 13 (2023) 100100.
[3] D.S. Sundaram, P. Puri, V. Yang, A general theory of ignition and combustion of nano- and micron-sized aluminum particles, Combust. Flame 169 (2016) 94–109.
[4] R.A. Yetter, G.A. Risha, S.F. Son, Metal particle combustion and nanotechnology, Proc. Combust. Inst. 32 (2) (2009) 1819–1838.

[5] H. Keck, C. Chauveau, G. Legros, S. Gallier, F. Halter, New experimental method for the simultaneous determination of concentration and size profiles of condensed combustion products around a burning aluminum droplet, Combust. Flame 268 (2024) http://dx.doi.org/10.1016/j.combustflame.2024.113616.
[6] E.L. Dreizin, Experimental study of aluminum particle flame evolution in normal and micro-gravity, Combust. Flame 116 (3) (1999) 323–333.
[7] Z. Li, N. Wang, B. Shi, S. Li, R. Yang, Effects of particle size on two-phase flow loss in aluminized solid rocket motors, 2019, pp. 33–40, http://dx.doi.org/10.1016/j.actaastro.2019.03.022, Vol. 159, book section 33.
[8] E.L. Dreizin, On the mechanism of asymmetric aluminum particle combustion, Combust. Flame 117 (4) (1999) 841–850.
[9] S. Gallier, A. Braconnier, F. Godfroy, F. Halter, C. Chauveau, The role of thermophoresis on aluminum oxide lobe formation, Combust. Flame 228 (2021) 142–153.
[10] J. Glorian, S. Gallier, L. Catoire, On the role of heterogeneous reactions in aluminum combustion, Combust. Flame 168 (2016) 378–392.
[11] Y. Gan, L. Qiao, Combustion characteristics of fuel droplets with addition of nano and micron-sized aluminum particles, Combust. Flame 158 (2) (2011) 354–368, http://dx.doi.org/10.1016/j.combustflame.2010.09.005.
[12] F. Halter, V. Glasziou, H. Keck, G. Legros, C. Chauveau, Experimental investigation of ignition temperatures of aluminum particles, in: 13th United States National Combustion Meeting, College Station, TX, 2023.
[13] C. Kong, D. Yu, S. Li, Q. Yao, Mechanism and modelling of aluminium nanoparticle oxidation coupled with crystallisation of amorphous Al2O3 shell, Combust. Theory Model. 20 (2) (2016) 296–312, http://dx.doi.org/10.1080/13647830.2015.1130266.
[14] R. Friedman, A. Maček, Ignition and combustion of aluminium particles in hot ambient gases, Combust. Flame 6 (1962) 9–19.
[15] B.J. McBride, NASA Glenn Coefficients for Calculating Thermodynamic Properties of Individual Species, Tech Rep TP-2002-211556, NASA, 2002.
[16] J.L. Prentice, Combustion of pulse-heated single particles of aluminum and beryllium, Combust. Sci. Technol. 1 (5) (1970) 385–398.
[17] J.L. Prentice, Aluminum Droplet Combustion: Rates and Mechanisms in Wet and Dry Oxidizers, Report, Naval Weapons Center, China Lake, CA, 1974.
[18] A. Zenin, G. Kusnezov, V. Kolesnikov, Physics of aluminum particle combustion at ultrasonic levitation, in: 39th Aerospace Sciences Meeting and Exhibit, in: Aerospace Sciences Meetings, American Institute of Aeronautics and Astronautics, Reno, NV, 2001.
[19] A. Zenin, G. Kusnezov, V. Kolesnikov, Physics of alumimum particle combustion at zero-gravity, in: 37th Aerospace Sciences Meeting and Exhibit, in: Aerospace Sciences Meetings, American Institute of Aeronautics and Astronautics, Reno, NV, 1999.
[20] E.L. Dreizin, Experimental study of stages in aluminium particle combustion in air, Combust. Flame 105 (4) (1996) 541–556.
[21] A.V. Tyurin, N.A. Gribchenkova, V.N. Guskov, K.S. Gavrichev, Thermodynamic properties of aluminum oxynitride from 0 to 340 K, Inorg. Mater. 51 (4) (2015) 340–344.
[22] S. Gallier, A physical model for the prediction of aluminum oxide residues, Int. J. Energ. Mater. Chem. Propuls. 23 (TBD) (2024) 1–15.
[23] N. Jüngst, Z. Wu, C. Ruan, M. Aldén, Z. Li, Light extinction and scattering to determine nanoparticle formation rates during droplet jetting in aluminum dust flames, Powder Technol. 453 (2025) http://dx.doi.org/10.1016/j.powtec.2025.120633.
[24] A. Braconnier, Étude Expérimentale De La Combustion D'une Particule D'aluminium Isolée : Influence De La Pression Et De La Composition De L'atmosphère Oxydante (Thesis), 2020.